JOURNAL OF SOLID STATE CHEMISTRY **124,** 205–213 (1996)
ARTICLE NO. 0227

Synthesis and Characterization of New Hydrotalcite-like Compounds Containing Ni(II) and Mn(III) in the Hydroxide Layers and of Their Calcination Products

C. Barriga,* J. M. Fernández,* M. A. Ulibarri,*,[1] F. M. Labajos,† and V. Rives†

*Dpto. de Química Inorgánica e Ingeniería Química, Facultad de Ciencias, Universidad de Córdoba, 14004, Córdoba, Spain; and
†Dpto. de Química Inorgánica, Universidad de Salamanca, 37008, Salamanca, Spain

Received August 1, 1995; in revised form February 28, 1996; accepted March 21, 1996

Two nickel–manganese hydroxycarbonates with Ni/Mn ratios close to 2/1 (Ni2Mn) and 3/1 (Ni3Mn) have been synthesized by coprecipitation under an air atmosphere from aqueous solutions of Ni(II) and Mn(II). Characterization by powder X-ray diffraction, transmission electron microscopy, and differential thermal and thermogravimetric analyses confirm a hydrotalcite-like structure for these brown colored compounds, indicating that Mn(II) is at least partially oxidized to Mn(III) during the synthesis process. Thermal decomposition in air at 450°C leads to formation of NiO as the major product in both samples. At 700°C, the Ni/Mn ratio determines the nature of the nickel–manganese mixed oxides present, in addition to NiO. Temperature-programmed reduction of calcined samples indicate that the major mixed oxide in sample Ni2Mn calcined at 700°C is ilmenite, $NiMnO_3$, while in Ni3Mn it is the spinel $NiMn_2O_4$. At 1000°C, formation of NiO and $NiMn_2O_4$ spinel occurs whichever the Ni/Mn ratio in the starting material.

INTRODUCTION

Hydrotalcite, the mineral $[Mg_6Al_2(OH)_{16}]CO_3 \cdot 4\ H_2O$, has been taken as a reference name for many other isomorphous materials. They are also referred to as anionic clays, and as such form a complementary class of materials to conventional cationic silicate clays.

Hydrotalcite-like compounds can be represented by the general formula $[M(II)_{1-x}M(III)_x(OH)_2]^{x+}\ A^{z-}_{x/z} \cdot nH_2O$, with $M(II)$ = Mg, Zn, Ni, Cu, ... , $M(III)$ = Al, Fe, Cr, ... , and $A^{z-} = CO_3^{2-}, SO_4^{2-}, Cl^-, \ldots$. Their structure consists of brucite-like layers, $Mg(OH)_2$, with $M(II)$/$M(III)$ substitution in octahedral sites of the hydroxide sheet, resulting in a net positive charge which is neutralized by the interlayer anions; water molecules also exist between the layers (1–3). These materials have found a great variety of uses as such or after calcination at high temperatures (4–8).

Calcination of these compounds at temperature depending on the particular cations in the layers and anions in the interlayer leads to mixed oxides characterized by structural homogeneity and the absence of chemical segregation (9, 10). Hydrotalcites are consequently a set of precursors useful for the preparation of catalytically active oxides (11–13). The activity and selectivity of these solids have been established for several reactions (14–17).

Although most of the papers published on this type of materials correspond to these containing two main groups cations (i.e., Mg–Al) or with one transition metal cation (Mg–Fe, Ni–Al, ...), very few papers report on hydrotalcite-like materials containing two transition metal cations in the layers (Co–Fe, Ni–Fe, ...) (18–20).

In this paper we report on preparation of hydrotalcite-like compounds with Ni and Mn in the hydroxide layers. With a wide range of attainable oxidation states, Mn has been valued as a component of batteries but also of industrial catalysts of oxidative processes (including conversion of hydrocarbons and the oxidative coupling of methane) and in reductive catalysis, as a promoter in combination with other transition metals (21–23).

The synthesis has been carried out by coprecipitation of Ni(II) and Mn(II) cations at room temperature with strongly alkaline solutions. As already reported for Mg–Mn hydrotalcites (24, 25), during precipitation Mn(II) ions undergo partial oxidation to Mn(III), giving rise to mixed layered hydroxides with the hydrotalcite structure. The changes induced by thermal treatment also have been studied. Finally, the nature of mixed oxides obtained by calcination at increasing temperatures has been assessed from X-ray diffraction and temperature programmed reduction.

[1] To whom all the correspondence should be sent.

0022-4596/96 $18.00

EXPERIMENTAL

Synthesis of the Samples

Synthesis of the hydroxycarbonates was carried out by dropwise addition (during a period of 3 h) of 100 ml of a solution containing $Ni(NO_3)_2 \cdot 6H_2O$ (0.08 *M*) and $MnCl_2 \cdot 2H_2O$ (0.04 *M*) to 100 ml of a 0.2 *M* NaOH, 0.1 *M* Na_2CO_3 solution for the so-called ''Ni2Mn'' samples, the number indicating the integer closest to the Ni/Mn atomic ratio; for the ''Ni3Mn'' samples the Ni(II) and Mn(II) salt concentrations were 0.09 and 0.03 *M*, respectively. The precipitate thus obtained was centrifuged and washed several times with distilled, deionized water, until no infrared band due to nitrate was detected; a final washing with acetone was also performed, in order to eliminate excess water. The solid was finally dried in an oven at 60°C.

Characterization

The Ni/Mn ratio was determined by atomic absorption spectroscopy (AAS) using a Perkin–Elmer 3100 apparatus after dissolution of the samples in diluted HCl and adding H_2O_2 to reduce all Mn to Mn(II). Carbon analysis was carried out in a Perkin–Elmer 2400 CHN analyzer. Powder X-ray diffraction (PXRD) diagrams were obtained with a Siemens D500 instrument, using Cu$K\alpha$ radiation (graphite monochromator) at a scanning speed of 2°(2θ)/min. Transmission electron micrographs (TEM) were obtained in a JEOL 200CX microscope. The Fourier-transform infrared spectra (FT-IR) of the samples were recorded in a Perkin–Elmer FT-IR 1730 apparatus, with a nominal resolution of 2 cm^{-1} and averaging 100 scans; the sample was pressed in KBr pellets with 3 mg sample per 100 mg KBr; under the experimental conditions used, FT-IR absorption bands with a transmittance larger than 1–2% were detected. Differential thermal analysis (DTA) and thermogravimetric analysis (TG) were recorded on Perkin–Elmer DTA 1700 and TGS-2 instruments, respectively, using flowing air or nitrogen (60 ml $\cdot$ min^{-1}) at a heating rate of 12°C $\cdot$ min^{-1}. Specific surface areas of the samples prepared have been measured by the single-point method using a Micromeritics Flowsorb II 2300 instrument, using a N_2/He (30/70) gas mixture from Sociedad Española de Oxígeno (SEO, Spain). Temperature-programmed reduction (TPR) analysis was carried out in a Micromeritics TPR/TPD 2900 instrument, at a heating rate of 10°C $\cdot$ min^{-1}, and using ca. 10 mg of sample and a H_2/Ar (5% vol) mixture as reducing agent (60 ml $\cdot$ min^{-1}); experimental conditions for TPR runs were chosen according to procedures reported elsewhere (26) in order to attain good resolution of component peaks.

RESULTS AND DISCUSSION

Hydrotalcite-like Materials

Chemical analysis results for both samples are given in Table 1. The Ni/Mn ratios were close to the values of the starting solutions, and small variations are within experimental error in most of the cases.

X-ray diffraction patterns of both samples are shown in Fig. 1. The overall aspect of the diagrams indicates a layered structure, peaks due to higher order diffraction being observed at 7.68, 3.88, and 2.66 Å for Ni2Mn and at 7.81, 3.89 and 2.66 Å for Ni3Mn. In addition, both samples show the characteristic doublet at 1.54 and 1.51 Å. The better crystallinity (sharper peaks) of sample Ni2Mn compared with sample Ni3Mn should be noted. The first three peaks (at lower 2θ values) are due to diffraction by planes (003), (006), and (009), while the doublet is originated by planes (110) and (113), respectively. The positions are very close to those reported in the literature for hydrotalcite (3), takovite (Ni–Al hydroxycarbonate) (10), and desautelsite (Mg–Mn hydroxycarbonate) (24, 25). The (0*hk*) diffraction lines are extremely broad and tailing toward higher 2θ values as observed in other hydrotalcite-like materials synthesized following the coprecipitation method (25). On the other hand, although the low crystallinity of the patterns, especially for Ni3Mn, does not permit us to rule out the presence of amorphous, unidentified materials, their content would be rather low, according to data obtained by subsequent techniques. As expected, a slight decrease in the (001) spacings is observed as the electric layer charge is increased, i.e., when the Ni/Mn atomic ratio decreases. The values for the positions of these (001) peaks arise within the range reported in the literature for hydrotalcite-like materials containing carbonate anions in the interlayer

TABLE 1
Metal Contents Data and Surface Area for Ni2Mn and Ni3Mn Samples and Their Calcined Products

Sample	%[a] Ni	%[a] Mn	Ni/Mn[b]	S^c_{BET}
Ni2Mn	37.3	16.7	2.09	70
Ni2Mn/125	39.0	17.9	2.04	80
Ni2Mn/450	48.8	22.5	2.02	58
Ni2Mn/700	50.5	22.9	2.04	15
Ni2Mn/1000	51.1	24	2.00	<1
Ni3Mn	41.7	11.8	3.08	70
Ni3Mn/125	46.6	14.3	3.05	72
Ni3Mn/450	56.7	17.2	3.08	56
Ni3Mn/700	60.8	18.0	3.13	17
Ni3Mn/1000	60.8	18.3	3.07	4

[a] wt%.
[b] atomic ratio.
[c] $m^2 \cdot g^{-1}$.

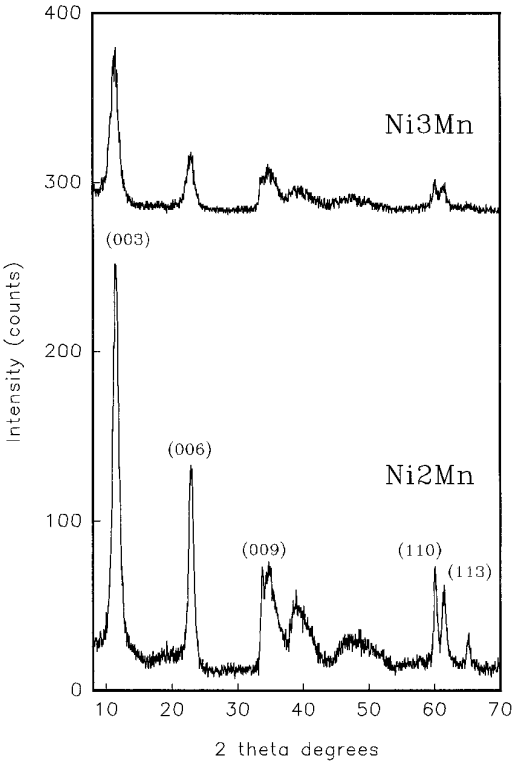

FIG. 1. PXRD diagrams of untreated Ni2Mn and Ni3Mn hydrotalcite-like materials.

(3, 4, 25), assuming a thickness of 4.8 Å for the brucite-like layers; it should be noted that the ionic radii of the cations in hydrotalcite (Mg(II) 0.86 Å, Al(III) 0.67 Å) are fairly close to those of the cations here existing (Ni(II) 0.83 Å, Mn(II) 0.97 Å, Mn(III) 0.78 Å) (27).

The *a* dimension can be calculated (6) from the position of the (110) peak at 3.08 Å. These findings confirm the hydrotalcite-like structure of the materials synthesized, and so the (at least partial) oxidation of Mn(II) to Mn(III) during synthesis.

For these anionic clays, the negative charge of the interlayer anions should balance the positive charge in excess (due to the trivalent cations) in the brucite-like layers. Chemical analysis for C indicates a content of 1.66% for sample Ni2Mn; this value corresponds to 91% of Mn being Mn(III). That is within experimental error and it can be concluded that almost all Mn has been oxidized to the trivalent state during synthesis. Such an oxidation has been previously reported (24, 25) for Mg–Mn hydrotalcites and explained on the basis of the larger relative stability of the Mn(III) oxidation state than Mn(II) at high pH values (24). With regards to sample Ni3Mn, the C content was 1.29, corresponding to the presence of all Mn as Mn(III). However, determination of the oxidation state of Mn solely from carbon content ignores the possible presence of bicarbonate species, as well as of lattice defects and/or species in brucite-like layers formed via acid/base reaction of the hydroxyl groups, leading to O^{2-} or H_2O species in the layers. In order to overcome this ambiguity, the TPR profiles of the untreated Ni2Mn and Ni3Mn samples have been recorded. Hydrogen consumption for sample Ni2Mn was 7.74 mmol H_2/g solid, and for sample Ni3Mn it was 8.18 mmol H_2/g solid. We have previously shown that Ni(II) in hydrotalcites is quantitatively reduced to Ni(0), while reduction of Mn(n) ($n >$ II) goes only to Mn(II), which is not further reduced to the metallic state (28). In order to test the nature of the species existing after the TPR run, we have recorded the PXRD diagram of the residue obtained after the TPR of sample Ni2Mn, showing lines due to Ni(0) and MnO, thus confirming the above mentioned final oxidation states for these two metals.

From the chemical analysis data for Ni and Mn content in samples Ni2Mn and Ni3Mn, total hydrogen consumption expected for reduction processes Ni(II) → Ni(0) and Mn(III) → Mn(II) are 7.87 and 8.18 mmol H_2/g solid, respectively. These values are in agreement, within experimental error, with the values experimentally recorded for a Mn(III) content of 91 and 100% for samples Ni2Mn and Ni3Mn, respectively, thus confirming the results obtained from the C chemical analysis.

The TEM micrographs of the samples show agglomerates of small particles (Fig. 2), and they are slightly larger for sample Ni2Mn than for sample Ni3Mn, in agreement with the better crystallinity observed by X-ray diffraction for the former sample. However, this increase in the particle size seems to be insufficient to give rise to noticeable differences in the specific surface areas of the samples, the values of which are also included in Table 1.

The DTA profiles (recorded in air and in nitrogen) for sample Ni3Mn are shown in Fig. 3. Both profiles show two strong, sharp endothermic peaks at 209 ± 1°C (due to dehydration) and 302 ± 1°C (dehydroxylation and decarboxylation). Ascription of these peaks to the named processes has been made according to previous data (10, 24) corresponding to similar samples to those studied here. The traces in both experiments are slightly different above 400°C, showing a weak, broad, ill-defined exothermic effect centered at ca. 580°C when the analysis is performed in air, together with a clearly detected endothermic effect at 782°C for the same experiment. The presence of a low intensity exothermic effect (only when the analysis is performed in air) immediately after decomposition of the hydroxycarbonate can be associated to oxidation reactions, as already observed in other hydrotalcites containing oxidizable cations, such as Mn(III) to Mn(IV) (24) and Co(II) to Co(III) (29). The TG traces, also included in the same figure, show a multiple, overlapped, weight loss in the temperature range 100–750°C, making uncertain any calculation leading to determination of the water content, as removal of interlayer molecular water cannot be differenti-

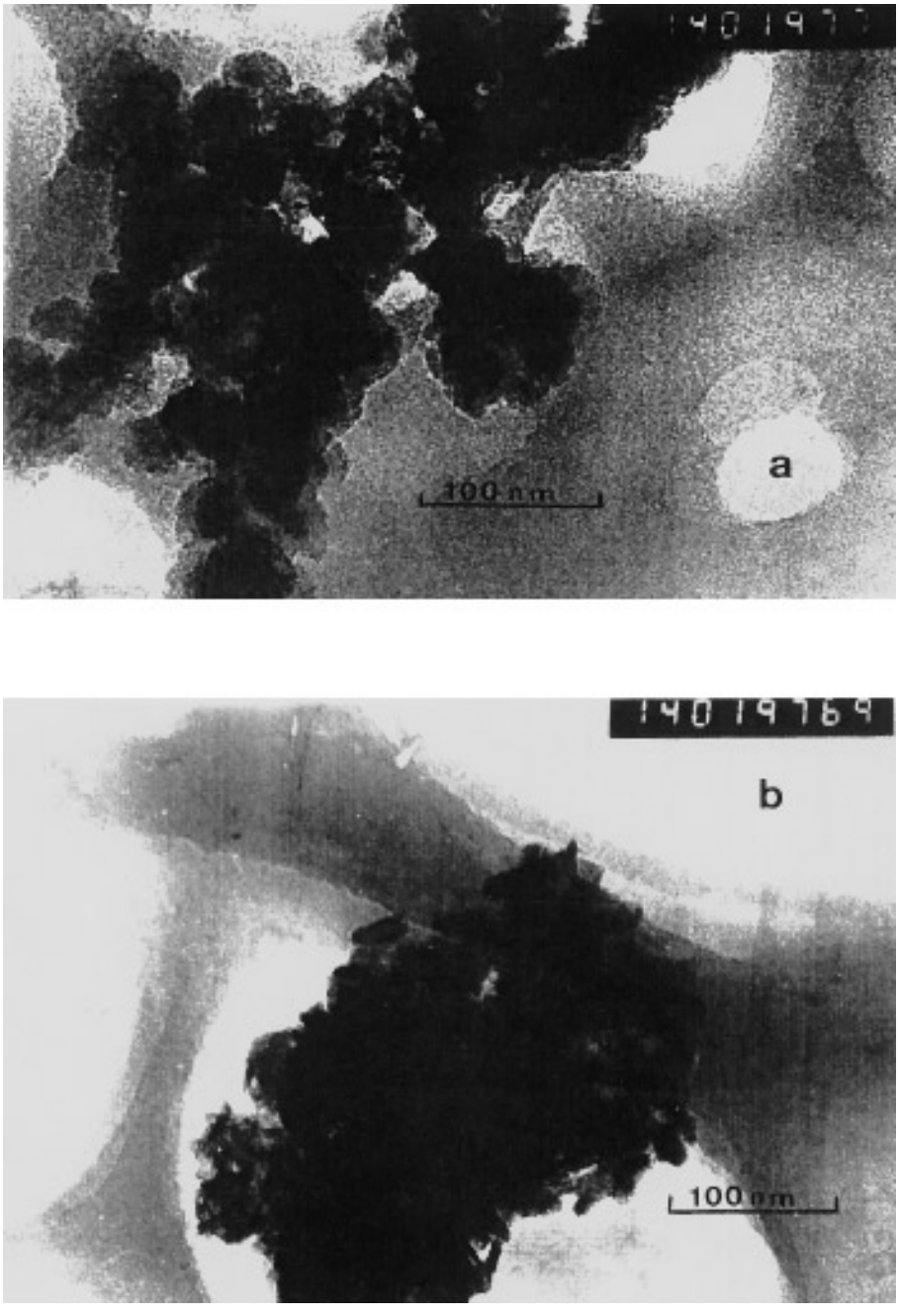

FIG. 2. TEM of the original samples: (a) Ni2Mn and (b) Ni3Mn.

ated from dehydroxylation and decarboxylation. Nevertheless, the total weight loss under air (25%) is lower than when the analysis is performed under nitrogen (31.5%), in agreement with the oxidation process above mentioned.

The behavior shown by Ni2Mn sample during TG/DTA experiments was rather similar to that above and the figures have not been included to avoid repetition.

The FT-IR spectrum for sample Ni3Mn is shown in Fig. 4 (the spectrum for sample Ni2Mn is very similar and has been omitted). The broad band at ca. 3420 cm^{-1} is due to ν_{OH} mode of hydroxyl groups, both from the brucite-like layers and from the hydroxyl groups of water molecules existing in the interlayer space, for which δ_{HOH} is recorded at 1637 cm^{-1}. Bands due to interlayer carbonate are also observed. Thus, the split band with maxima at 1400 and 1358 cm^{-1} is ascribed to mode ν_3 (antisymmetric stretching) of carbonate species, recorded as a single band at 1450 cm^{-1} for free CO_3^{2-} species, but which splits because of the

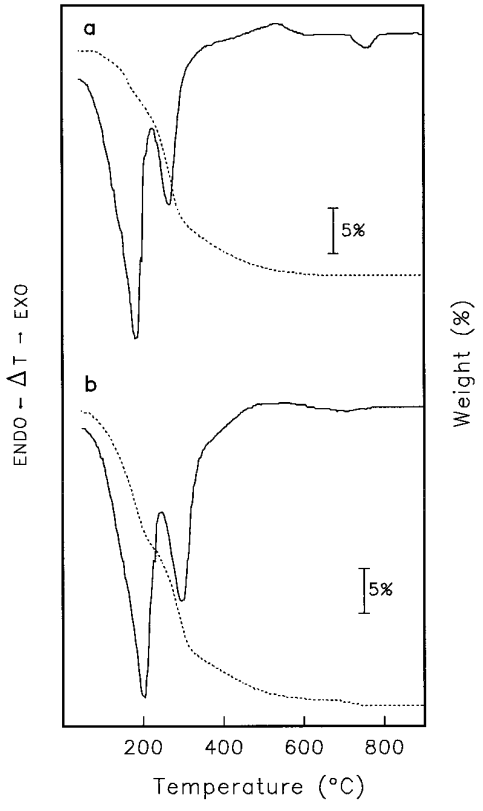

FIG. 3. TG and DTA profiles of Ni3Mn (a) in air and (b) in nitrogen.

lowering symmetry and hydrogen bonding with hydroxyl groups in the interlayer space. Additional confirmation of this carbonate–hydroxyl hydrogen bonding arises from the weak shoulder at 3075 cm^{-1} (30). In addition, restricted symmetry in the interlayer space gives rise to activation of carbonate mode ν_1, which is recorded as a weak shoulder at 1060 cm^{-1}, as previously reported for other hydrotalcites (31). No infrared evidence could be recorded of the presence of bicarbonate species, which could be formed due to the lowering in pH during washing of the precipitates, thus displacing toward the right the equilibrium

$$CO_3^{2-} + H_2O \rightarrow HCO_3^- + OH^-.$$

The other bands in the FT-IR spectrum below 1000 cm^{-1} can be ascribed to lattice modes of the brucite-like layers (31).

Calcined Products

We have analyzed the crystalline phases existing in the samples after calcination at increasing temperatures. We have chosen calcination temperatures from information provided by the DTA results. The samples were calcined at 150°C (just before dehydration), 450°C (after dehydroxylation/decarboxylation), 700°C (before the endothermic effect recorded in air and ascribed to oxidation/reduction processes), and 1000°C, where well crystallized phases are expected to be formed. Samples will be named Ni2Mn/*T* or Ni3Mn/*T*, where *T* stands for the calcination temperature, in °C. The XRD patterns of samples Ni2Mn and Ni3Mn calcined in air are included in Fig. 5. The layered structure is stable up to 150°C, although a decrease of the interlayer spacing and crystallinity is observed; both effects can be ascribed to a loss of interlayer water during the calcination treatment. The slight increase in the specific surface area (see Table 1) can be ascribed to formation of small craters on the brucite-like layers, through which dehydration occurs (9).

The PXRD diagrams of samples calcined at 450°C show that for both samples the layered structure of the hydrotalcite collapses, leading to formation of NiO (rock-salt structure). Together with diffraction lines due to NiO, weak diffraction peaks appear due to mixed oxides, which structure and stoichiometry (as well as the oxidation state of manganese) depend on the nature of the starting material. So, while for samples Ni2Mn these lines could be ascribed to ilmenite, $NiMnO_3$ (Fig. 5a), for sample Ni3Mn lines at 4.8, 2.9, and 2.5 Å due to the spinel structure (Ni_2MnO_4 or $NiMn_2O_4$) can be observed in addition to the lines corresponding to NiO (Fig. 5b). Nevertheless, the low crystallinity of the material (diffraction lines very broad and rather weak) makes rather uncertain the exact determination of the manganese oxides existing in these samples, as already observed for other calcined hydrotalcites (24). The FT-IR spectra of the samples calcined at 450°C (Fig. 4) show weak bands at 3420, 1400, and 1358 cm^{-1} due to residual hydroxyl and carbonate groups, together with lattice vibrations in

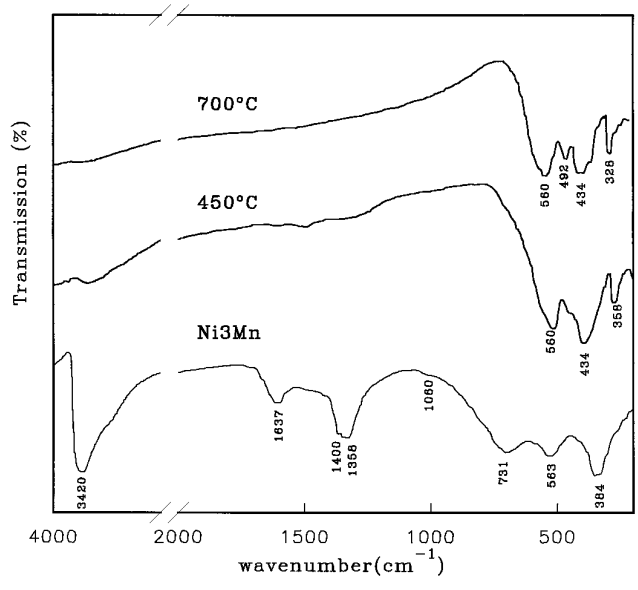

FIG. 4. FT-IR spectra of Ni3Mn. Original and calcined in air for 3 h at different temperatures.

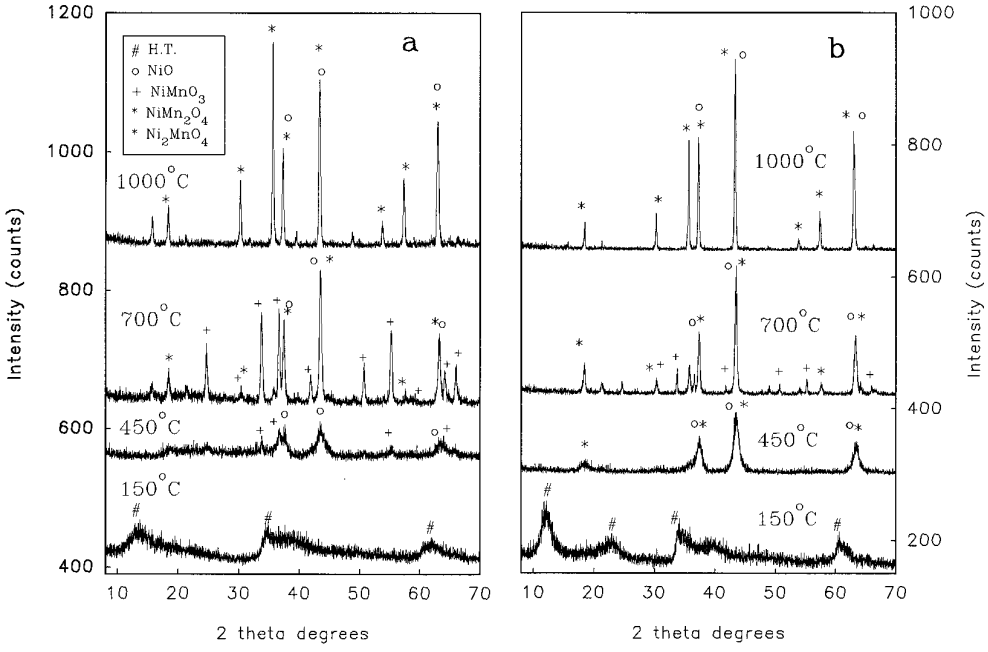

FIG. 5. PXRD diagrams of (a) Ni2Mn and (b) Ni3Mn calcined in air for 3 h at different temperatures.

the 800–250 cm^{-1} range (30). The PXRD diagram of sample Ni2Mn calcined at 700°C, Fig. 5a, corresponds to a mixture of rock-salt NiO and of ilmenite, $NiMnO_3$, although weak peaks due to the spinel phases are also observed. The PXRD diagram for sample Ni3Mn calcined at the same temperature, Fig. 5b, also shows the presence of NiO as the major Ni-containing phase, but Mn is mostly incorporated into the spinel, and weak lines corresponding to ilmenite also appear.

Formation of ilmenite takes place through a further oxidation of manganese ions from Mn(II) (in the starting soluble salts) to Mn(III) (during the precipitation process to yield the hydrotalcite-like structure), and to Mn(IV) during calcination, in agreement with the exothermic effect recorded in the DTA profile at ca. 580°C when the analysis is performed in air (Fig. 3a). On the other hand, formation of NiO in addition to ilmenite, $NiMnO_3$, is expected taking into account the value of the Ni/Mn ratio, larger than 1.0.

The FT-IR spectra of samples calcined at 700°C (Fig. 4) shows exclusively well-defined absorption bands in the 800–250 cm^{-1} range, while bands due to carbonate and hydroxyl groups have been completely removed, in agreement with total elimination of carbonate and hydroxyls at this temperature.

In order to obtain additional information about the thermal stability of the different phases formed during calcination, PXRD diagrams of samples calcined at 700°C during different heating times have been recorded. It should be stressed that at this temperature all carbonate and hydroxyl groups have been removed, and so all changes are due to reaction between Ni and Mn oxides. These diagrams are given in Fig. 6 for samples Ni2Mn and Ni3Mn, calcined at 700°C in air for 6, 15, and 30 h. For sample Ni2Mn, all diffraction lines due to spinel (existing when the sample is calcined at this temperature, but for 3 h, see Fig. 5a) have disappeared, and all diffraction lines recorded can be ascribed to NiO and $NiMnO_3$. As the calcination time is increased, the intensities of the ilmenite lines, with respect to those of NiO, decrease; however, no new lines develop, thus suggesting that these changes are due to a differential recrystallization of both phases, and not to an increase in the relative amount of NiO with respect to $NiMnO_3$. The behavior shown by sample Ni3Mn is, however, rather different. When calcination at 700°C is prolonged, the stable phases formed are NiO and a Ni–Mn spinel ($NiMn_2O_4$ or Ni_2MnO_4), the relative intensities of the lines originated by both phases being maintained as the calcination time is increased; only a sharpening of the lines is being observed, probably due to improved crystallinity of the particles. Chemical analysis data in Table 1 indicate that, as expected, the Ni/Mn atomic ratio is maintained close to 3.0, and hence, formation of the spinel Ni_2MnO_4 cannot be safely ignored. However, the larger content of NiO, as concluded from the PXRD diagrams (see Fig. 6b) suggests formation of the spinel $NiMn_2O_4$, together with NiO.

It should also be noted that formation of the inverse spinel Ni_2MnO_4 would require location of Ni(II) both in octahedral and tetrahedral sites, while in ilmenite $NiMnO_3$, both cations Ni(II) (d^8) and Mn(IV) (d^4) are located in octahedral sites. From the electronic configurations, crystal

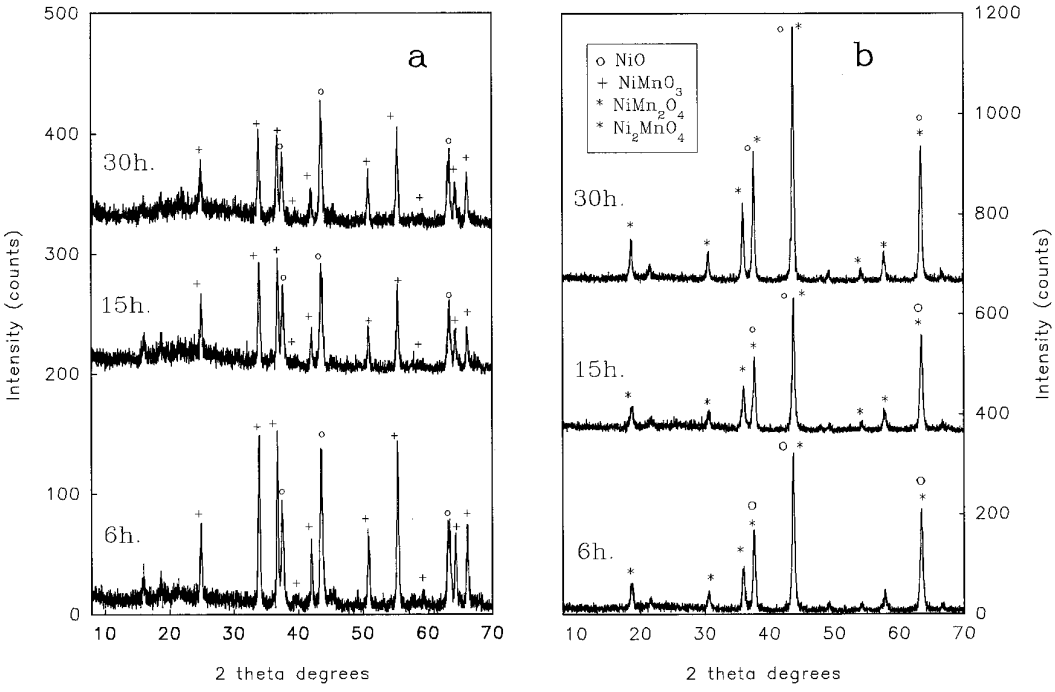

FIG. 6. PXRD diagrams of (a) Ni2Mn and (b) Ni3Mn calcined in air at 700°C for 6, 15, and 30 h.

field stabilization energies are larger, in both cases, for octahedral coordination. Thus, we can conclude that in the presence of Mn(IV), formation of ilmenite is favored vs formation of inverse spinel Ni_2MnO_4. For sample Ni3Mn, ilmenite is formed as an intermediate product (and also as a minor component) when the sample is calcined at 700°C, but vanishes as the calcination time is increased, leading to formation of a more stable phase at this temperature, probably spinel $NiMn_2O_4$, containing Mn(III).

When the samples are calcined at higher temperatures (1000°C), PXRD shows that only spinel and NiO are formed, although the relative intensities of the lines corresponding to both phases are different indicating that the spinel content is larger for sample Ni2Mn (larger intensity of the diffraction line at 2.53 Å due to planes (311) not coincident with any peak of NiO), although for sample Ni3Mn calcined at 1000°C, NiO is the major phase. As expected, and confirmed by the atomic absorption data collected in Table 1, the Ni/Mn ratio is maintained along the calcination process, thus accounting for the larger NiO content in sample Ni3Mn than Ni2Mn calcined at 1000°C.

A point remaining obscure is the nature of the spinel formed, $Ni_2^{II}Mn^{IV}O_4$ or $Ni^{II}Mn_2^{III}O_4$; this can be hardly discerned, due to the closeness of the diffraction peaks in both cases, and to the fact that some of the lines coincide with those of the major component, NiO. However, it should be noted that no peaks due to any other phase containing manganese are detected and, at least for the high temperature calcined samples, formation of any other phases would be rather easily detected by PXRD, due to sintering of the materials at a so high calcination temperature. Therefore, for calcined products obtained from Ni2Mn, formation of Ni_2MnO_4 can be discarded, as the atomic Ni/Mn ratio of 2.0 coincides, within experimental error, with that determined by atomic absorption. Therefore, no NiO would crystallize. However, rock-salt NiO obviously has formed. As formation of $NiMnO_3$ (containing Mn(IV)) has been observed at medium calcination temperatures, formation of spinel $NiMn_2O_4$ (containing Mn(III)) requires Mn(IV) → Mn(III) reduction, which could account for the weak endothermic effect recorded at 782°C, and also would explain the presence of NiO in the product calcined above 782°C. This behavior is rather similar to that previously reported for other hydrotalcites (18, 20, 24), for which calcination leads to formation of a single oxide of the divalent cation (Ni in our case), together with mixed oxides the precise nature of which depends on the nature of the cations existing in the brucite-like layers. The above discussion permits us to propose the formation of the spinel $NiMn_2O_4$.

With regards to the nature of the spinel formed from the Ni3Mn sample, TPR analysis of samples calcined at 700 and 1000°C has been carried out since, as mentioned above, determination of the precise oxidation state of manganese is hardly attained from the PXRD diagrams, as diffraction lines are coincident (within experimental error) for, at least, two different spinel, i.e., $NiMn_2O_4$ and Ni_2MnO_4.

As an example, TPR curves for sample Ni2Mn previously calcined at 700 and 1000°C are given in Fig. 7. Reduction of sample Ni2Mn/1000 takes place in better defined steps, with maxima at ca. 410 and 500°C, while for sample Ni2Mn/700 reduction starts at a lower temperature, reaching a maximum at ca. 350°C, with a clearly detected shoulder at ca. 470°C.

The total hydrogen consumption during reduction (12.27 and 10.94 mmol H_2/g solid for samples Ni2Mn/700 and Ni2Mn/1000, respectively) can be split into the amount of hydrogen required for a quantitative reduction of Ni(II) to Ni(0), the remaining amount of hydrogen being consumed for reduction of manganese; hence, from knowledge of the final oxidation state for manganese (as concluded from the PXRD analysis performed on the residue), the average oxidation state of manganese in the starting material can be calculated. Sample Ni2Mn/700 contains 8.60 mmol Ni/g and 4.17 mmol Mn/g (Table 1). Assuming an oxidation state of +4 for Mn and +2 for Ni, reduction to Mn(II) and Ni(0) would require consumption of 12.77 mmol H_2/g solid, a value only 4% larger than that experimentally recorded. For sample Ni2Mn/1000 (containing 8.71 mmol Ni/g and 4.37 mmol Mn/g), however, such a reduction process would require 13.08 mmol H_2/g solid, i.e., 20% larger than that recorded. But if it is assumed that Mn exists as Mn(III), total hydrogen consumption for reduction to Ni(0) and Mn(II) would consume 10.90 mmol H_2/g solid, a value coincident with that recorded.

We conclude that in sample Ni2Mn/700 most of manganese exists as Mn(IV), in agreement with the PXRD data, showing diffraction lines due to ilmenite, $NiMnO_3$. For sample Ni2Mn/1000, however, PXRD data confirm the presence of a spinel, that, according to TPR data, should be $NiMn_2O_4$ (where Mn exists as Mn(III)), and not Ni_2MnO_4 (containing Mn(IV)).

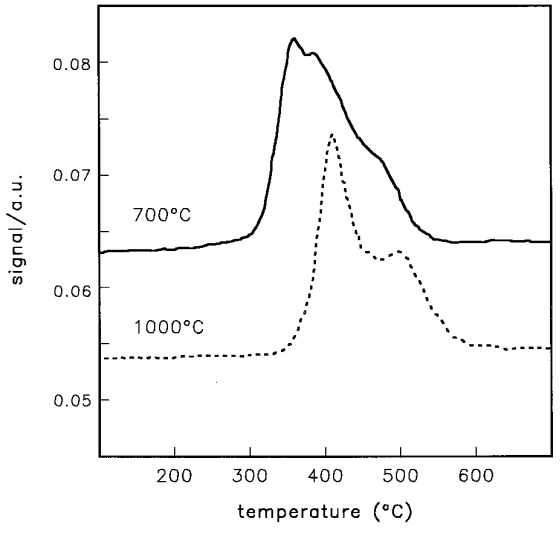

FIG. 7. TPR profiles of Ni2Mn calcined in air for 3 h at 700 and 1000°C.

With regard to samples Ni3Mn/700 and Ni3Mn/1000, hydrogen consumptions were 12.12 and 12.74 mmol H_2/g solid, respectively. These values correspond, within experimental error (1% and 5%, respectively) with the expected values assuming Mn existing in the +3 state, i.e., as spinel $NiMn_2O_4$. This conclusion is in agreement with the information provided by the PXRD analysis above: the ilmenite content in sample Ni3Mn/700 is very low, and disappears as the calcination time is increased up to 3 h; for sample Ni3Mn/1000, PXRD data indicate the presence of the spinel.

Summarizing the above information about the calcination of the samples at increasing temperatures, the following scheme can be assumed to explain thermal decomposition in air of Ni2Mn and Ni3Mn hydrotalcites:

$$\text{Ni2Mn(HT)} \xrightarrow{150^\circ\text{C}} \text{Ni2Mn (HT)} \xrightarrow{450^\circ\text{C}} \text{NiO} + \text{NiMnO}_3 \xrightarrow{700^\circ\text{C}}$$
$$\xrightarrow{700^\circ\text{C}} \text{NiO} + \text{NiMnO}_3 + (\text{NiMn}_2\text{O}_4) \xrightarrow{1000^\circ\text{C}} \text{NiO} + \text{NiMn}_2\text{O}_4$$
$$\text{Ni3Mn(HT)} \xrightarrow{125^\circ\text{C}} \text{Ni3Mn(HT)} \xrightarrow{450^\circ\text{C}} \text{NiO} + \text{spinel} \xrightarrow{700^\circ\text{C}}$$
$$\xrightarrow{700^\circ\text{C}} \text{NiO} + \text{NiMn}_2\text{O}_4 + (\text{NiMnO}_3) \xrightarrow{1000^\circ\text{C}} \text{NiO} + \text{NiMn}_2\text{O}_4.$$

CONCLUSIONS

When Mn(II) and Ni(II) are simultaneously precipitated under an air atmosphere from aqueous solutions using NaOH and Na_2CO_3 (aq), Mn(II) is oxidized to Mn(III) and a solid possessing the hydrotalcite-like structure is obtained, with Ni(II) and Mn(III) ions in the layers, the Ni/Mn atomic ratio depending on the relative concentrations of the cations in the starting solutions. The Ni/Mn ratio strongly determines the nature of crystalline phases formed during prolonged calcination of these solids: calcination of Ni2Mn at 700°C leads to formation of NiO and $NiMnO_3$, while calcination of Ni3Mn at the same temperature leads to formation of NiO and $NiMn_2O_4$ (spinel). However, calcination at 1000°C leads to formation of NiO and $NiMn_2O_4$ spinel, regardless of the Ni/Mn atomic ratio in the starting material.

ACKNOWLEDGMENTS

The authors are thankfull for financial support from project CICYT (MAT93-787) and Junta de Castilla y León (Consejería de Cultura y Turismo). Thanks are also given to Mr. A. Montero and Ms. M. C. Mohedano for their help in obtaining some of the experimental results. This work is within the Concerted European Action on Pillared Layered Solids (CEA-PLS).

REFERENCES

1. R. Allmann, *Acta Crystallogr. Sect. B* **24,** 792 (1986).
2. H. F. W. Taylor, *Mineral. Mag.* **39,** 377 (1973).
3. S. Miyata, *Clays Clay Miner.* **23,** 369 (1975).
4. D. L. Bish, *Bull. Mineral.* **103,** 170 (1980).
5. S. Miyata and T. Hirose, *Clays Clay Miner.* **26,** 441 (1978).
6. F. Cavani, F. Trifirò and A. Vaccari, *Catal. Today* **11,** 173 (1991).
7. T. Sato and A. Okuwaki, *Solid State Ionics* **45,** 43 (1991).
8. M. A. Ulibarri, I. Pavlovic, M. C. Hermosín, and J. Cornejo, *Appl. Clay Sci.* **10,** 131 (1995).
9. W. T. Reichle, S. Y. Kang, and D. S. Everhardt, *J. Catal.* **101,** 352 (1986).
10. M. J. Hernández, M. A. Ulibarri, J. L. Rendón, and C. J. Serna, *Thermochim. Acta* **81,** 311 (1984).
11. E. C. Kruissink, L. L. van Reijen, and J. R. H. Ross, *J. Chem. Soc., Faraday Trans. I* **77,** 649 (1981).
12. O. Clause, B. Rebours, E. Merlen, F. Trifirò, and A. Vaccari, *J. Catal.* **133,** 231 (1992).
13. R. Spinicci and M. A. Ulibarri, *Mater. Chem. Phys.* **26,** 1 (1990).
14. W. T. Reichle, *J. Catal.* **94,** 547 (1985).
15. E. Suzuki, M. Okamoto, and Y. Ono, *J. Mol. Catal.* **61,** 283 (1990).
16. A. Corma, V. Fornés, R. M. Martín-Aranda, and F. Rey, *J. Catal.* **134,** 58 (1992).
17. J. Valim, B. M. Karinki, J. King, and W. Jones, *Mol. Cryst. Liq. Cryst.* **211,** 271 (1992).
18. A. Mendiboure and R. Schöllhorn, *Rev. Chem. Minér.* **23,** 819 (1986).
19. K. el Malki, A. de Roy, and J. P. Besse, *Eur. J. Solid State Inorg. Chem.* **26,** 339 (1989).
20. H. C. B. Hansen, C. B. Koch, and R. M. Taylor, *J. Solid State Chem.* **113,** 46 (1994).
21. R. Burch and S. C. Tsang, *Appl. Catal.* **65,** 259 (1989).
22. R. W. Judd, C. Komodromos, and T. J. Reynolds, *Catal. Today* **13,** 237 (1992).
23. E. M. Gottschalk and G. J. Hutchings, *Appl. Catal.* **55,** 127 (1989).
24. J. M. Fernández, C. Barriga, M. A. Ulibarri, F. M. Labajos, and V. Rives, *J. Mater. Chem.* **4,** 1117 (1994).
25. H. C. B. Hansen and R. M. Taylor, *Clay Miner.* **26,** 507 (1991).
26. P. Malet and A. Caballero, *J. Chem. Soc., Faraday Trans. I* **84,** 2369 (1988).
27. J. E. Huheey, ''Inorganic Chemistry: Principles of Structure an Reactivity,'' 4th ed., p. 114. Harper, Cambridge, MA, 1983.
28. V. Rives, M. A. Ulibarri, and A. Montero, *Appl. Clay Sci.* **10,** 83 (1995).
29. M. A. Ulibarri, J. M. Fernández, F. M. Labajos, and V. Rives, *Chem. Mater.* **3,** 626 (1991).
30. F. M. Labajos, V. Rives, and M. A. Ulibarri, *J. Mater. Sci.* **27,** 1546 (1992).
31. M. J. Hernández-Moreno, M. A. Ulibarri, J. L. Rendón, and C. J. Serna, *Phys. Chem. Miner.* **12,** 34 (1985).